Revisiting Thermal Analysis of Hypereutectic Spheroidal Graphite Cast Irons

M.J. CASTRO-ROMÁN, J. LACAZE, A. REGORDOSA, J. SERTUCHA, and R. DEL CAMPO-CASTRO

This study deals with early solidification of hypereutectic cast irons at varying carbon content and roughly constant alloying additions. Thermal analysis of such alloys shows that the start of the eutectic reaction occurs at a nearly constant temperature for mildly hypereutectic compositions. A similar trend is observed with more hypereutectic compositions but at a higher starting temperature. This jump in the start temperature of the eutectic reaction has not been previously evidenced and is here addressed by considering primary precipitation of graphite. Limiting the analysis to spheroidal graphite cast irons, it is demonstrated that simulation of primary graphite precipitation based on a 2D nucleation/lateral growth model allows substantiating the experimental distinction found between mildly and highly hypereutectic cast irons. This modeling explains that highly hypereutectic alloys start eutectic solidification in a limited temperature range that is nearly insensitive to the initial carbon equivalent of the alloy and to inoculation. This approach also suggests that the start of the eutectic solidification of mildly hypereutectic cast irons is shifted to lower temperature until growth of austenite enriches the liquid in carbon to such an extent that growth of graphite becomes possible.

https://doi.org/10.1007/s11661-020-06005-7

I. INTRODUCTION

IN cast iron foundry shops, thermal analysis (TA) has slowly evolved over the years as an essential tool for melt control before pouring, but also as a predictive tool of microstructure and casting properties. The possibilities of thermal analysis have been often reviewed, *e.g.,* in the recent works by Dioszegi *et al.*[1] and Stefanescu.[2–4] TA is expected first to give the so-called carbon equivalent, CE, which is used to locate hypoeutectic alloys with respect to the austenite-graphite eutectic but much more has been looked for, *e.g.,* graphite shape and inoculation level. In practice, foundries rely on experimental calibration of their processing route and state that an alloy behaves as eutectic when the corresponding thermal record shows one single plateau that encompasses the whole solidification process.[5] However, results by Chaudhari *et al.*[6] have long ago demonstrated that mildly hypereutectic alloys may show eutectic-type records while being of varying CE. This behavior could result from the solidification conditions in the TA cup, while other microstructures could be revealed in parts with varying size and cooling rate cast with such a melt, thus generating some confusions.

As a matter of fact, the conditions for growth of graphite and austenite are affected by tiny changes in the process parameters, *e.g.,* melt composition, graphite nucleation, and growth or else cooling rate. Accepting that growth of austenite is easier than that of graphite, graphite growth is thus the key in understanding TA records as it is for analyzing the microstructure of cast iron parts. In the literature, the basic knowledge of graphite growth was largely obtained in relation to the eutectic reaction, while little research has been done on the primary growth of graphite, *i.e.,* the precipitation of graphite alone directly from the liquid. Rare studies on primary growth have been carried out by quenching samples during solidification or by investigating the microstructure of highly hypereutectic alloys.[7,8] There is also one outstanding experimental work based on TA analysis including highly hypereutectic cast irons which is of main concern for the present study. This work was performed over several years and led to two final contributions dedicated to the possibility of extending thermal analysis for predicting as-cast microstructure of

M.J. CASTRO-ROMÁN and R. DEL CAMPO-CASTRO are with the Cinvestav Unidad Saltillo, Av. Industria Metalúrgica 1062, Parque Industrial Saltillo-Ramos Arizpe, Ramos Arizpe, Coahuila, C.P. 25900, Mexico. J. LACAZE is with the CIRIMAT, Université de Toulouse, 31030 Toulouse, France. Contact e-mail: jacques.lacaze@ensiacet.fr A. REGORDOSA and J. SERTUCHA are with the Azterlan, Basque Research Technological Alliance, Aliendalde Auzunea 6, 48200 Durango, Bizkaia, Spain.

Manuscript submitted June 14, 2020.
Article published online September 28, 2020

industrial cast irons[9] and laboratory alloys.[6] There were two essential outputs from this work which are as follows: (i) the thermal records of mildly hypereutectic cast irons often show one single eutectic plateau and (ii) in the highly hypereutectic composition range, the thermal records may show an arrest which corresponds to primary deposition of graphite.

The aim of the present work is to relate graphite precipitation with the features of the TA records for mildly and hypereutectic alloys. It will be shown that making use of equilibrium phase diagram is of definite help for a better understanding of cast iron solidification. For achieving this aim, the first part of this contribution is dedicated to analyzing the results by Chaudhary *et al.*[6,9] as well as more recent results with emphasis put on hypereutectic alloys. A number of clear features are obtained which are then discussed in the second part with the support of a simple modeling approach applied to primary spheroidal graphite precipitation. This leads to a tentative conclusion on the reason for the difficulty in controlling mildly hypereutectic spheroidal graphite cast irons by thermal analysis.

II. CHARACTERISTIC SOLIDIFICATION TEMPERATURES AND THEIR DEPENDENCE ON CARBON EQUIVALENT

A. *TA Records from Chaudhari et al.[6]*

The so-called eutectomer samples used by Chaudhari *et al.*[6] were cylinders 40 mm in diameter and 60 mm in length, weighing 680 g. Castings were carried out with (i) untreated base melts, (ii) after Ni-Mg alloy addition for spheroidization but no inoculation or post-inoculation, (iii) and after the same spheroidization treatment and post-inoculation. Before casting, the melts were maintained for a while at a high temperature of 1510 °C to 1538 °C to ensure obtaining the liquid cooling part of the cooling curve. The carbon equivalent CE of the melts was modified by changing both carbon and silicon contents and was expressed as $CE = w_C + w_{Si}/3$, where w_i is the alloy content in element i (wt pct). The spheroidizing treatment led to a 0.4 to 1.7 wt pct (0.85 wt pct on average) addition of nickel to the cast irons for a final Mg content of 0.042 to 0.067 wt pct.

The series of thermal records for base melts and for Ni-Mg-treated alloys showed similar features which are illustrated in Figure 1 in the case of the Ni-Mg-treated alloys. Note that the original curves were copies of the chart records with the time increasing from right to left. The curves were also shifted along the time axis so that they could be arranged in order of ascending value of CE, from left to right. After picking up the data from the original figure, the temperature was converted from Fahrenheit to Celsius for drawing Figure 1. Hypoeutectic irons showed a prolonged primary liquidus arrest which corresponds to formation of austenite and was denoted T_{AL}. Generally, this arrest was not of the recalescent type and its temperature gradually decreased with increasing CE as shown with the downwards dashed arrow labeled T_{AL} in Figure 1. This initial arrest is followed by a eutectic plateau at a temperature that can be associated either to the stable system or to the metastable system. For these hypoeutectic alloys, Chaudhari *et al.*[6] noticed that the transition from the austenite thermal arrest to the eutectic plateau was smooth, which they understood as indicating that there was no appreciable amount of eutectic forming before the eutectic plateau.

For mildly hypereutectic alloys with CE in the range from 4.26 to 4.60 wt pct, solidification is expected to start with precipitation of graphite. However, for these alloys, a thermal arrest similar to the austenite liquidus arrest was observed at a temperature lower than the equilibrium eutectic temperature, T_{EUT}, but higher than that of the eutectic plateau. An example is the bold blue record of alloy #1309 (CE = 4.55 wt pct) in Figure 1. Chaudhari *et al.* suggested to call it "initial eutectic arrest," T_{EN}, hence implicitly assuming that the eutectic reaction started with this arrest. As graphite was assumed to have already appeared because of the hypereutectic composition, this arrest must correspond to the formation of austenite.

With increase in CE beyond 4.60 wt pct, a primary liquidus arrest corresponding to precipitation of pro-eutectic graphite was observed. This latter arrest was associated with considerable recalescence (up to 5.5 °C) and its duration was up to 15 seconds. The temperature of this arrest rose steeply with the CE value as shown with the upwards dashed arrow labeled T_{LG} in Figure 1. This was considered by Chaudhari *et al.*[6] as a proof that a graphite liquidus can occur on a cooling curve. Upon further cooling, all four records for highly hypereutectic alloys showed a T_{EN} arrest and then a eutectic plateau at a temperature corresponding to the stable system. According to Chaudhari *et al.*, the T_{EN} arrest rises slightly with increase of the CE value as illustrated with the corresponding dashed arrow in Figure 1.

The third series of alloys prepared by Chaudhari *et al.*,[6] *i.e.,* the hypereutectic Ni-Mg-treated and inoculated alloys, showed the same kind of features as above with the exception of the graphite liquidus arrest which was not observed even for highly hypereutectic alloys. The authors felt that this absence was due to the fact that the increased number of nuclei "was able to control the precipitation of graphite from the melt" which may be translated to "nucleation of graphite was more regular in inoculated alloys". However, the same authors also reported records with a graphite liquidus arrest for highly hypereutectic commercial cast irons which had been spheroidized with a Fe-Si-Mg (FSM) alloy and inoculated.[9] In any case, one of the conclusions drawn by Chaudhari *et al.* from their experimental campaigns is that the solidification of hypoeutectic, eutectic and strongly hypereutectic alloys is readily identifiable with TA, while records for mildly hypereutectic alloys show uncertain variability which is further detailed below. Clarifying this issue appeared quickly as an important aim when we started the present work.

B. *Characteristic Temperatures from Chaudhari et al.[6,9]*

When analyzing their results, Chaudhari *et al.*[6] reported the temperature of the thermal arrests as

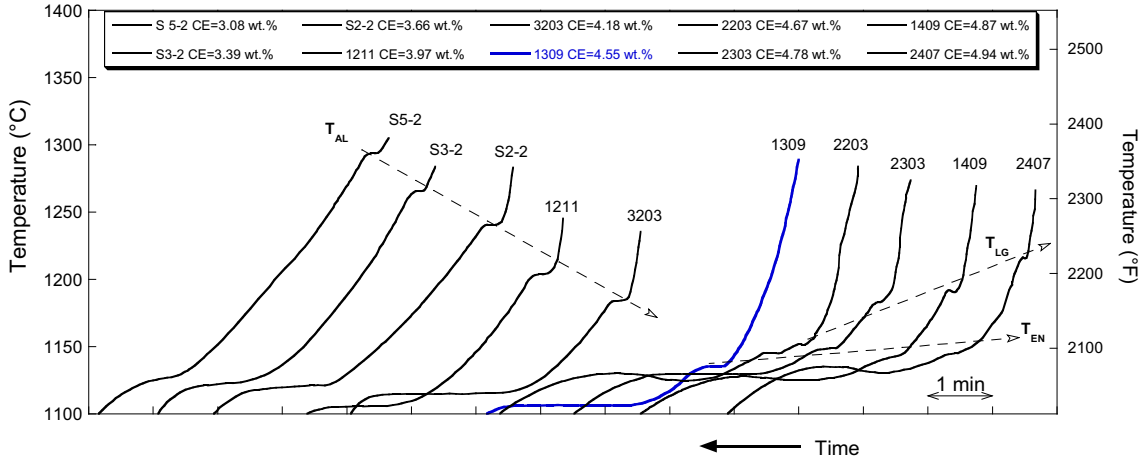

Fig. 1—Cooling curves at increasing CE value (from left to right) of Ni-Mg-treated but not-inoculated Fe-C-Si alloys of various carbon and silicon contents. Adapted from Chaudhari *et al.*[6]

function of the alloy CE values. However, the silicon content of their alloys was varied in a large range—from 1.06 to 2.84 wt pct—when it is known that the austenite and graphite liquidus as well as the eutectic temperature all change with the silicon content. Noticing that all their hypereutectic alloys had a silicon content higher than 2.40 wt pct, it appeared of interest for further analysis to first select only alloys with such silicon content, *i.e.,* with silicon content within the limited range in between 2.40 and 2.84 wt pct. Available data fulfilling this condition encompass a few hypo-eutectic alloys and untreated alloys, but these were mainly hypereutectic spheroidized industrial alloys[9] and laboratory alloys.[6] Tables A-I and A-II in Appendix A list the reference of all the alloys that were selected for analysis, also including their carbon and silicon contents as well as a few microstructure information for those alloys that were spheroidized. The values of the characteristic temperatures reported below are those that were written along the records in the papers by Chaudhari *et al.* which were then converted to Celsius.

The carbon equivalent CE which was used by Chaudhari *et al.*[6,9] is expected to take a value of 4.26 wt pct at the eutectic composition. However, the assessment of the Fe-C diagram which is presently accepted[10] indicates that the eutectic is at 4.34 wt pct. This difference is certainly to be related to the kinetics aspects of thermal analysis as opposed to equilibrium.[5] Furthermore, the expression $CE = w_C + w_{Si}/3$ which was selected by Chaudhari *et al.* goes against current knowledge of the Fe-C-Si phase diagram which indicates a lower coefficient for silicon.[2,11,12] It is proposed here to analyze the results of Chaudhari *et al.* by properly locating their alloys with respect to equilibrium phase diagram. Based on an assessment of the Fe-C-Si phase diagram,[13] a linearization of the austenite liquidus, T_L^{γ}, and graphite liquidus, T_L^{g}, for silicon content up to 3 wt pct has been previously proposed.[12] This linearization was extended to account for addition of several elements up to 1 wt pct for most of them. Limited to the alloys considered in the present work that could contain some Cu, Mn and Ni, the following equations apply:

$$T_L^{\gamma} = 1576.3 - 97.3 \cdot w_C - 4.08 \cdot w_{Cu} - 5.66 \cdot w_{Mn} - 7.86 \cdot w_{Ni} - 23.0 \cdot w_{Si} \quad [1]$$

$$T_L^{g} = -534.7 + 389.1 \cdot w_C + 40.62 \cdot w_{Cu} - 2.40 \cdot w_{Mn} + 18.421 \cdot w_{Ni} + 113.2 \cdot w_{Si} \quad [2]$$

The eutectic trough is then obtained at the intersection of these two liquidus surfaces. From this, the carbon equivalent according to this description of the phase diagram writes:

$$CE_{99} = w_C + 0.092 \cdot w_{Cu} + 0.007 \cdot w_{Mn} + 0.054 \cdot w_{Ni} + 0.28 \cdot w_{Si} \quad [3]$$

The carbon content at the eutectic, w_C^{eut}, is such that $CE_{99} = 4.34$ wt pct. The equilibrium eutectic temperature, T_{EUT}, is thus obtained by inserting w_C^{eut} in either of the above liquidus expressions:

$$T_{EUT} = 1154.02 + 4.86 \cdot w_{Cu} - 5.00 \cdot w_{Mn} - 2.60 \cdot w_{Ni} + 4.246 \cdot w_{Si} \quad [4]$$

The values of the first arrest detected on the cooling curves reported by Chaudhari *et al.*[6,9] for alloys with silicon content higher than 2.40 wt pct are plotted in Figure 2 as function of CE_{99}. There are four points for hypoeutectic alloys, two base melts and two after Ni-Mg treatment, while all other results are for hypereutectic alloys. The first arrest for hypoeutectic alloys is T_{AL}, while for hypereutectic alloys only arrests corresponding to T_{LG} are reported in Figure 2. The solid lines represent the calculated austenite and graphite liquidus

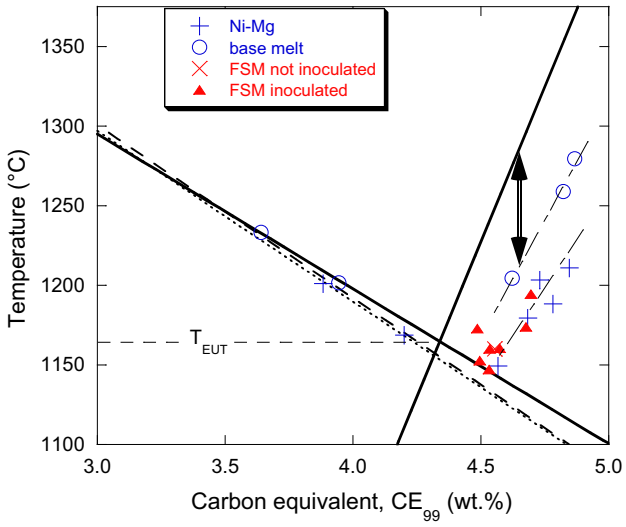

Fig. 2—Values of the first arrest on the cooling curves as function of CE_{99} for laboratory not-inoculated alloys[6] and FSM-treated industrial alloys[9] with silicon content between 2.40 and 2.84 wt pct. The solid lines are the austenite and graphite liquidus (Eqs. [1] and [2] at 2.6 wt pct Si); their intersection at CE_{99} = 4.34 wt pct represents the eutectic point in the Fe-C isopleth section. Dotted and short dashed lines show the austenite liquidus according to Eqs. [5] and [6], respectively. The two dashed lines have been drawn through the available data for hypereutectic base melts and Mg-treated alloys, respectively. The double arrow shows how is defined the undercooling ΔT_L^{gra} with respect to graphite liquidus.

(Eqs. [1] and [2]) for w_{Si} set at an average value of 2.6 wt pct Si and no Ni.* Please note that these liquidus lines are metastable below the equilibrium eutectic temperature T_{EUT}.

*Owing to the simultaneous change in CE_{99}, the liquidus lines when accounting for the addition of Ni are practically superimposed to those shown in Figure 2 and have thus not been plotted.

On the hypoeutectic side, Eq. [1] suggests that near-eutectic alloys present an undercooling of 5 °C to 10 °C with respect to the austenite liquidus, a value which is well within the range of values observed by Heine.[11] It appeared of interest to compare the austenite liquidus given by Eq. [1] to the expressions proposed by Chaudhari *et al.*[9] for the base alloys, $T_{AL,base}$, and for the Ni-Mg-treated alloys, $T_{AL,Ni\text{-}Mg}$:

$$T_{AL,base} = 2929 - 195.7 \cdot w_C - 42.6 \cdot w_{Si}[°F] = 1609.4 - 108.7 \cdot w_C - 23.7 \cdot w_{Si}[°C] \quad [5]$$

$$T_{AL,Ni-Mg} = 2927 - 193.4 \cdot w_C - 49.0 \cdot w_{Si} + 132.9 \cdot w_{Mg}[°F] = 1608.3 - 107.4 \cdot w_C - 27.2 \cdot w_{Si} + 73.8 \cdot w_{Mg}[°C] \quad [6]$$

These expressions have been drawn in Figure 2 with short dashed (Eq. [5]) and dotted (Eq. [6]) lines, setting the silicon content at 2.6 wt pct and the magnesium content at 0.05 wt pct. It is seen that these two interrupted lines are nearly superimposed to each other and do fit nicely with the experimental results for hypoeutectic alloys.

In the hypereutectic range, the liquidus arrests show a high undercooling with respect to the equilibrium graphite liquidus. This undercooling, which will be denoted ΔT_L^{gra}, is illustrated with the double arrow in Figure 2. It can be noted that the undercooling below the graphite liquidus is nearly twice as large for Mg-treated alloys as for base melts. It is worth further stressing that the fact the Mg-treated alloys had been inoculated or not does not appear to significantly change this undercooling. Accordingly, this much higher undercooling shown by the spheroidized alloys must be related to graphite growth kinetics. This is what is expected: growth of lamellar graphite is much quicker than growth of spheroidal graphite, hence the lower ΔT_L^{gra} undercooling detected on thermal records of base melts. A dashed line has been drawn in Figure 2 through each of the two series of data, *i.e.,* those for base melts and those for spheroidized alloys. They are both nearly parallel to the graphite liquidus indicating that the arrest occurred at nearly constant undercooling whatever the carbon equivalent of the alloys was.

The next step in the analysis of the thermal records reported by Chaudhari *et al.*[6,9] was to consider the eutectic arrest limiting our investigation to hypereutectic spheroidized alloys. This has been done first with the same series of alloys as those selected for Figure 2, *i.e.,* with Si content higher than 2.4 wt pct. As described by these authors, the eutectic reaction may show either a single plateau or a double plateau (see Figure 1). A double plateau was observed for not-inoculated alloys with a pre-eutectic reaction T_{EN} followed by a decrease in temperature to reach the minimum temperature, T_{EU}, at which the bulk eutectic reaction takes place. Only the T_{EN} arrest was considered here as indicating the start of the pre-eutectic reaction. For inoculated alloys, there was a single plateau on the records and thus only the T_{EU} temperature was reported. The results are plotted in Figure 3 with open symbols for T_{EN} values and solid symbols for T_{EU} values.

In Figure 3 appears a jump of nearly 10 °C for the start of the eutectic reaction between mildly and strongly hypereutectic alloys. This was not pointed out by Chaudhari *et al.* and could be made evident here only by limiting the range of silicon contents. This will be supported by other results presented later in this section where the transition zone will also be detailed. What is seen in Figure 3 is that the formation of austenite for all highly hypereutectic alloys occurs at about 1146 °C which may be associated with a liquid at $CE_{99} \approx 4.53$ wt pct (upper horizontal arrow pointing to the left). The T_{EN} or T_{EU} temperature of mildly hypereutectic alloys (CE_{99} less than about 4.46 wt pct) corresponds to a temperature of 1136.5 °C which is then related to a liquid composition at $CE_{99} \approx 4.63$ wt pct (lower arrow pointing to the right).

In Figure 3, another observation was of concern which is that a pre-eutectic reaction T_{EN} did not show up for the mildly hypereutectic inoculated alloys. Such a

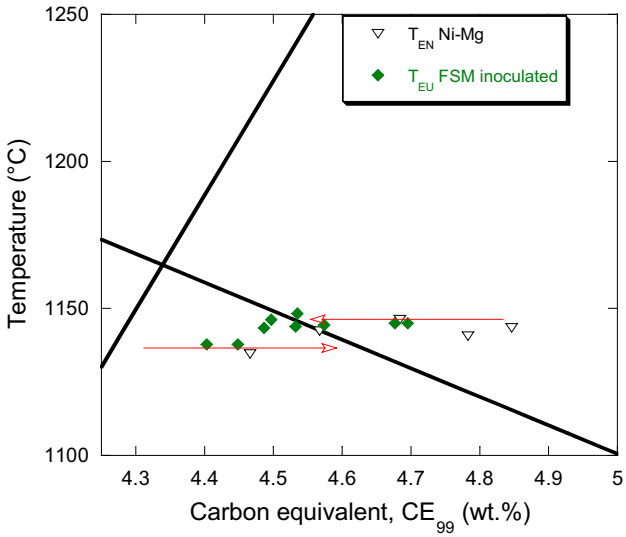

Fig. 3—Values of the first eutectic arrest, either T_{EN} (open symbols) or T_{EU} (solid symbols)[6,9] as function of CE_{99} for alloys with silicon content between 2.40 and 2.84 wt pct. The solid lines are the austenite and graphite liquidus (Eqs. [1] and [2]) calculated at 2.6 wt pct Si. In the caption, Ni-Mg is for laboratory alloys[6] while FSM stands for industrial alloys[9]

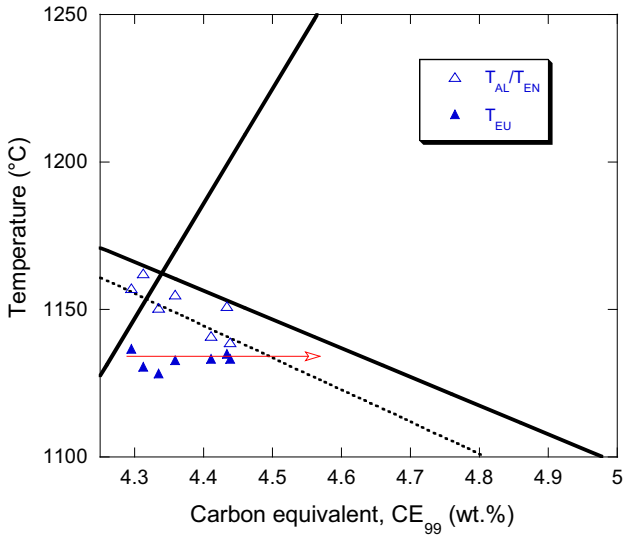

Fig. 4—Values of the T_{AL} or T_{EN} (open symbols) and of T_{EU} (solid symbols) arrests as function of CE_{99} for alloys with silicon content between 1.86 and 2.20 wt pct.[9] The bold solid lines are the austenite and graphite liquidus (Eqs. [1] and [2]) and the dotted line is the $T_{AL,base}$ austenite liquidus (Eq. [5]), all calculated at 2.0 wt pct Si. The red arrow is located at the same eutectic undercooling as in Fig. 3, $\Delta T_{EUT} = 28$ °C.

pre-eutectic arrest was, however, reported by Chaudhari *et al.* for most of their near-eutectic industrial alloys.[9] However, these latter alloys were not inoculated and then had a much lower silicon content than that of the alloys shown in Figure 3. Following the same way as before, alloys with silicon content between 1.86 and 2.20 wt pct were selected, see Table A-I for details. The results for the first arrest, either T_{AL} or T_{EN}, and the bulk eutectic arrest, T_{EU}, are reported in Figure 4. As expected, the temperature of the first arrest decreases when CE_{99} increases suggesting a continuity between T_{AL} for hypoeutectic alloys and T_{EN} for mildly hypereutectic alloys as they both relate to formation of austenite. Chaudhari *et al.*[9] noticed that "T_{EN} may be mistaken for T_{AL}, though the former should be considerably longer". This statement implies they were expecting some eutectic would form in hypereutectic alloys as soon as the austenite liquidus was reached, which has in fact been the basis of later modeling approaches of cast iron solidification. However, the records reported by Chaudhari *et al.* did not evidence any lengthening of the arrest when shifting from T_{AL} to T_{EN} implying that no appreciable amount of eutectic formed until some high enough undercooling was reached.

In Figure 4, it appears also that the temperature for the start of the bulk stable eutectic reaction for near-eutectic and mildly hypereutectic alloys is 26 °C to 34 °C below the equilibrium eutectic temperature. The red arrow pointing to the right has been located as in Figure 3 at 28 °C below the equilibrium eutectic to illustrate the similarity of this result for inoculated (Figure 3) and for not-inoculated (Figure 4) Mg-treated alloys. It is worth stressing that previous modeling approaches, *e.g.*, those by Lacaze *et al.*[14] and others,[15,16] that were based on the same understanding as proposed by Chaudhari *et al.*[6] and described above, predicted an increase of the bulk eutectic temperature with carbon equivalent (see the T_{EN} arrow in Figure 1). This expected increase is not consistent with experimental observations, suggesting that the modeling of solidification of hypereutectic alloys needs to be improved.

Another feature of the T_{AL} arrest in Figure 4 is that it shows a variable undercooling with respect to the austenite liquidus (Eq. [1]). The dotted line shows the T_{AL} calculated with Eq. [5] and it is seen that it gives the lower limit of the experimental values. The intersection with the arrow is at $CE_{99} = 4.49$ wt pct which corresponds to $CE = 4.60$ wt pct for these alloys at 2 wt pct Si. This latter value of CE is exactly the value obtained by Chaudhari *et al.* when performing a similar extrapolation. They associated this limit to the transition between mildly and highly hypereutectic alloys. Confusions may occur easily for the alloys in between the eutectic and this limit because T_{EN} may appear or not, and furthermore may show a variable undercooling when present.

Before analyzing further and discussing these findings in Section III, it was felt necessary to check the reproducibility of the experimental observations reported above with more recent data.

C. *Other Series of TA Records*

The first additional series that was considered deals with base melts which have not been spheroidized or inoculated, from which 24 high carbon hypereutectic alloys have been selected. The selected alloys have 1.70 to 1.91 wt pct Si and their chemical analysis showed they contained 0.14 to 0.24 wt pct Mn, 0.03 to 0.10 wt pct Cu and 0.021 to 0.045 wt pct P. The castings were performed at the experimental TQC foundry laboratory

(Spain) using standard thermal cups. According to the manufacturers of these cups and of the connecting wires, the standard deviation on the temperature reading is less than 2 °C. In the temperature range where primary precipitation of graphite could be expected, the cooling curves did not show any recalescent arrest, but a clear arrest marked by slope change. The temperature of this arrest was evaluated at the maximum of the first time derivative of the recorded cooling curves (see Figure 6 for an example). It was found to increase with the value of CE_{99} as shown in Figure 5 where have also been drawn the liquidus lines (Eqs. [1] and [2]) for an average composition of 1.80 wt pct Si, 0.19 wt pct Mn and 0.07 wt pct Cu. Also, the dashed line in Figure 5 has been located at the same ΔT_L^{gra} values as the line for base melts in Figure 2. A good agreement is thus seen between the two series of data, which supports the claim that this is effectively the graphite liquidus arrest that was recorded.

The T_{EU} values have also been plotted in Figure 5 and show exactly the same features as noticed in Figure 3, namely a jump between mildly and strongly hypereutectic alloys and a nearly constant T_{EU} temperature for strongly hypereutectic alloys. The difference with spheroidized alloys is that the eutectic reaction of highly hypereutectic alloys takes place at a eutectic undercooling of 6 °C only thus stressing the importance of primary graphite precipitation on the course of the solidification of cast irons.

Finally, a series of 36 industrial cast irons melts which have been spheroidized and pre-inoculated in the ladle was analyzed, again selecting alloys with silicon content in a limited range, namely 2.03 to 2.42 wt pct. They also contained 0.40 wt pct Cu and 0.47 wt pct Mn on average and the magnesium content was at 0.031 to 0.038 wt pct. These alloys were cast for thermal analysis

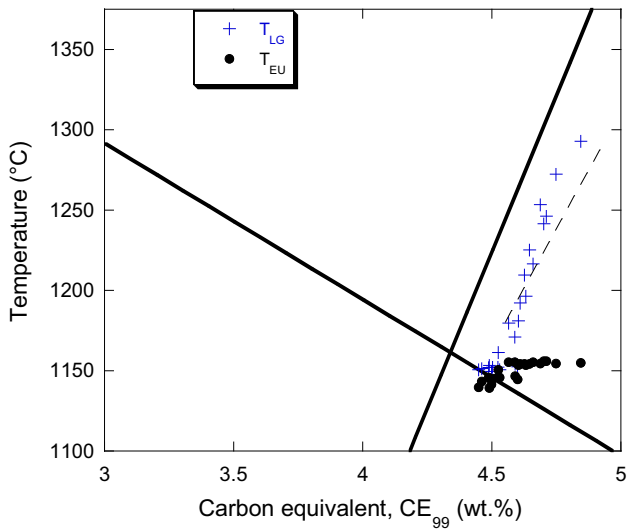

Fig. 5—Values of the T_{LG} (crosses) and T_{EU} (solid dots) arrests as function of CE_{99} for alloys with silicon content between 1.70 and 1.91 wt pct Si. The bold solid lines are the austenite and graphite liquidus (Eqs. [1] and [2]) calculated at 1.8 wt pct Si, 0.19 wt pct Mn and 0.07 wt pct Cu. The dashed line is positioned at the same undercooling with respect to the graphite liquidus as the one for base melts in Fig. 2.

either without post-inoculation or with 0.10 wt pct by weight of a commercial inoculant added at the bottom of the thermal cup. In this latter case, an increase of 0.075 wt pct in silicon was considered. The cups and recording equipment were the same as for the previous series. As an example, Figure 6 shows the TA record of two inoculated alloys, one at CE_{99} = 4.54 wt pct and the other at CE_{99} = 4.60 wt pct. For easing reading, this latter curve has been shifted along the time axis. Determining the characteristic temperature for the start of solidification was quite easy on these records by using the cooling rate, dT/dt, curve which has also been plotted in part in Figure 6. As a matter of fact, both cooling rate curves show a peak corresponding to the onset of solidification which has been indicated with a vertical interrupted line. For the alloy at lower CE_{99} value, the corresponding arrest is clearly of the T_{EN} type. For the more hypereutectic alloy, it corresponds to a slope change which indicates primary precipitation of graphite at T_{LG}. The second characteristic temperature on both of these records is the temperature T_{EU} at the minimum before the bulk eutectic plateau. This temperature has been indicated with an arrow pointing to the curve in Figure 6.

In Figure 7 has been plotted the T_{LG} temperature for those records showing it, and the T_{EU} temperature for all records of this second series. Some records in the range of CE_{99} values between 4.40 and 4.55 wt pct showed also a T_{EN} arrest which has not been shown to ease the description of the figure. The solid lines represent as before the austenite and graphite liquidus calculated for an average silicon content of 2.18 wt pct, 0.47 wt pct Mn and 0.39 wt pct Cu. Concerning the T_{LG} arrest, and for comparison, the dashed line for spheroidized alloys in Figure 2 has been located in Figure 7 at the same ΔT_L^{gra} values as in Figure 2. Seven of the crosses representing the T_{LG} arrest are quite close to this dashed line while three show smaller ΔT_L^{gra} value. On the whole, there is a good agreement between the present results

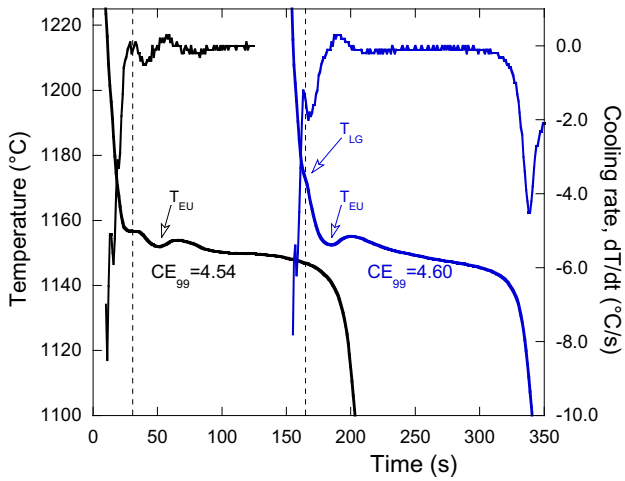

Fig. 6—Cooling curves of two spheroidized and inoculated alloys with CE_{99} at 4.54 and 4.60 wt pct. The vertical interrupted lines correspond to the local maximum on the cooling rate curves which relates to the start of solidification.

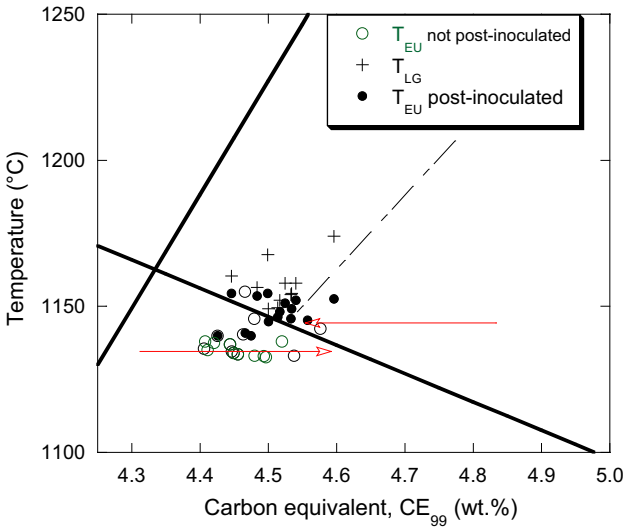

Fig. 7—Values of T_{LG} (plus signs) and T_{EU} (circles and dots) as function of CE_{99} for industrial alloys with silicon content between 2.03 and 2.42 wt pct Si. The bold solid lines are the austenite and graphite liquidus (Eqs. [1] and [2]) calculated at 2.18 wt pct Si, 0.47 wt pct Mn, and 0.39 wt pct Cu. The dashed line is at the same undercooling ΔT_L^{gra} as the one for spheroidized alloys in Fig. 2. The red arrows are located at the same eutectic undercoolings as in Fig. 3.

and those reported 45 years ago by Chaudhari *et al.*[6] The slightly lower values of ΔT_L^{gra} in the present series could well be expected as the amount of Mg was in the range 0.031 to 0.038 wt pct while it was reported at 0.042 to 0.067 wt pct by Chaudhari *et al.* (see Appendix A).

Concerning the eutectic reaction, the same jump in temperature from mildly to highly hypereutectic alloys as observed in Figure 3 is noticed in Figure 7 though there is also an overlapping zone. A well-defined transition zone is, however, observed in between CE_{99} = 4.45 wt pct and CE_{99} = 4.48 wt pct. For comparison, the upper and lower arrows have been positioned at the same eutectic undercoolings as in Figure 3. Most of the alloys which have not been post-inoculated show a T_{EU} temperature corresponding to the lower arrow, thus shifting the transition zone to higher CE_{99} values. Post-inoculated alloys with CE_{99} equal to or higher than 4.48 wt pct show a T_{EU} temperature which is slightly above the upper arrow as expected. Finally, there are two alloys with CE_{99} lower than 4.48 wt pct but showing high T_{EU} value which may illustrate uncertainty in chemical analysis (the standard deviation on carbon content is 0.05 wt pct) and possible variations in pre-inoculation efficiency.

According to the most generally accepted understanding of cast iron solidification, the set-up of the bulk eutectic reaction at T_{EU} depends essentially on the eutectic undercooling, namely when latent heat release becomes sufficiently rapid thanks to growth of both graphite and austenite.[4] On this basis, it was predicted that T_{EU} would increase continuously from hypoeutectic to mildly and then strongly hypereutectic alloys.[14] The above detailed analysis demonstrates that this conclusion is in contradiction with experimental information and thus that the basic assumption was not correct. The results for highly hypereutectic alloys in Figures 3, 5 and 7 suggest that an appropriate description of the formation of primary graphite had been missing in the previous modeling descriptions. This is the objective of the following discussion to provide an analysis that would allow retrieving the features described in this Section II.

III. DISCUSSION

This discussion is organized in two steps: i) calculation of the solidification path of highly hypereutectic alloys following two models for spheroidal graphite growth from the liquid and ii) consequences on the understanding of TA records for mildly hypereutectic spheroidal graphite cast irons.

A. *Modeling Primary Precipitation of Graphite*

Cooling and solidification of small castings such as eutectometer samples could be described quite satisfactorily considering the thermal gradients are small enough and thus assuming their temperature is homogeneous at any time. Hence, the following heat-balance equation applies:

$$A \cdot q = \rho^{\text{iron}} \cdot V \cdot C_p^{\text{iron}} \cdot \frac{\mathrm{d}T}{\mathrm{dt}} - \Delta H \cdot \frac{\mathrm{d}V^S}{\mathrm{dt}} \qquad [7]$$

where q is the density of the heat flux exchanged by the metal with the mold ($q < 0$ for usual casting conditions), V and A are the volume of the casting and its outer surface, respectively, V/A being the thermal modulus, ρ^{iron} and C_p^{iron} are the density and the heat capacity (per unit mass) of the metal, respectively, T is the sample temperature, ΔH is the latent heat of melting per unit volume, V^S is the solidified volume, and t is time.

It has been shown previously[12] that cooling and solidification of thermal cups may be described by setting q in Eq. [7] to the following expression:

$$q = -\sqrt{\Delta} \cdot \left(T - T^0\right) \cdot t^{-0.5} \qquad [8]$$

where Δ is defined by the properties of the cup and T^0 is the ambient temperature. This will be used here by inserting q in Eq. [7] with the value of the parameters as listed in Table I. They come from previous work[14] apart for Δ which has been adapted to thermal cups. It has been verified that the cooling rate at 1250 °C is of the order of the 3 °C/s mentioned by Chaudhari *et al.* All calculations will start at the pouring temperature of 1525 °C as an average of the holding temperature used by Chaudhari *et al.*[6] Only primary precipitation of spheroidal graphite will be considered, describing first the nucleation stage and then growth.

Nucleation kinetics has sometimes been described as a function of the cooling rate with a cooling rate-dependent coefficient fitted so as to retrieve the final nodule counts. Another approach describes nucleation as a

function of undercooling with respect to graphite liquidus, ΔT_L^{gra}, which expresses the actual driving force for graphite nucleation. This latter description must be coupled with the growth of the graphite phase to describe carbon desaturation in the liquid.[17] It is assumed that there exists in the liquid a distribution of potential nuclei that can be activated at increasing undercooling, see Dantzig and Rappaz[18] for a comprehensive description. New nuclei start being activated as soon as the temperature falls below the liquidus temperature and their number increases as the undercooling increases. However, if during cooling of the melt the undercooling ΔT_L^{gra} decreases because of the growth of graphite precipitates, nucleation of new particles stops. In this way, the effect of cooling rate on the number of nucleated graphite particles is closely related to growth of graphite precipitates as it should be. For the present work, we selected the simplest possible nucleation law which is written:

$$N_V = A_1 \cdot \Delta T_L^{gra} \quad [9]$$

where A_1 is a constant which depends on the inoculation treatment of the melt, and is thus a parameter that may be changed from one melt to another in relation to the amount of inoculant added. Such a law has been shown to be appropriate for analyzing continuous nucleation observed on samples quenched during directional solidification[19] and has been considered also in the analysis of *in situ* experiments followed with 4D-XRD.[20]

Growth of primary graphite precipitates will be described according to two models, a "classical" one which accounts for interfacial kinetics[17] and a more recent one which is based on a 2D nucleation/lateral growth of new layers at the outer surface of the spheroids.[21] The main features of these two models are reminded in Appendix B and their predictions described below. During cooling, a new class of nodules is generated at each time step of calculation according to Eq. [9]. These nodules then grow as described by either of the two growth models, leading to a decrease of the carbon content in the liquid which is estimated with the following approximate overall carbon balance:

$$V^0 \cdot \rho^{liquid} \cdot w_C^0 = V^{liquid} \cdot \rho^{liquid} \cdot w_C^{\infty} + V^{gra} \cdot \rho^{gra} \cdot w_C^{gra} \quad [10]$$

in which V^0, V^{liquid}, and V^{gra} are the initial volume, the volume of remaining liquid, and the volume of precipitated graphite; w_C^0 and w_C^{∞} are the initial carbon content in the alloy and the carbon content remaining in the liquid at time t, respectively; $w_C^{gra} = 100$ wt pct is the carbon content in graphite.

At any time, the volume of graphite that has precipitated is the sum of the volume of the nodules in all activated classes, and the change of graphite volume between two successive time steps may be inserted in Eq. [7] to calculate the related change in temperature. Calculations were carried out using the parameters in Table I and in appendix B for those specific to each growth model. The calculations were stopped when the extrapolation of the austenite liquidus below T_{EUT} was reached.

As expected from previous study,[14] the latent heat release during primary graphite growth leads only to a slight slope change which could hardly be seen on the calculated cooling curves. However, it could be inferred that an abrupt increase of graphite precipitation at some stage during primary precipitation explains the liquidus arrests reported in the previous section. Such an abrupt increase should lead to carbon desaturation of the liquid according to Eq. [10] and can thus be followed by drawing the solidification path, *i.e.,* the change in carbon content in the liquid w_C^{∞} with decreasing temperature. For a direct comparison with Figure 2, this is the change of $CE_{99} = w_C^{\infty} + 0.28 \cdot w_{Si}$ which will be plotted, and the calculations were carried out with w_{Si} set at 2.60 wt pct.

Figure 8 presents the calculations done with the "classical" growth model for Fe-C-Si alloys having CE_{99} at 4.6 , 4.7 and 4.8 wt pct. Preliminary calculations showed that values of A_1 set between 1 and 80 $mm^{-3}\ K^{-1}$ give nodule counts N_V varying between about 100 mm^{-3} and 4000 mm^{-3}, in agreement with the range of N_V values evaluated from the experimental information of Chaudhari *et al.* (see Appendix A). Figure 8(a) shows calculations made for CE_{99} = 4.8 wt pct and A_1 set to 1, 10, and 80 $mm^{-3}\ K^{-1}$. The predicted nodule count and fraction of graphite, g^{gra}, at the end of primary graphite precipitation are listed in Table II.

Upon cooling, the carbon content in the liquid first does not change and then suddenly decreases at a temperature that is higher and higher as A_1 increases. Once the carbon content has started to decrease, it may be noticed that the undercooling with respect to the graphite liquidus decreases also, meaning that nucleation of new nodules has stopped and only growth of the pre-existing nodules proceeds. The sudden curving of the solidification path may thus be associated with the thermal arrest observed on the TA records. It is further seen in Figure 8(a) that the solidification path hits the austenite liquidus at a temperature that is closer and closer to the eutectic temperature as the nucleation constant is increased. It is thus predicted a T_{EN} or T_{EU} value much closer to the stable eutectic temperature, T_{EUT}, than observed, see Figure 3.

In Figure 8(b), calculations for CE_{99} at 4.6, 4.7 and 4.8 wt pct were reported only for A_1 = 1 $mm^{-3}\ K^{-1}$ because the same features as above were observed for higher A_1 values. It is noted that the curving of the solidification path for A_1 = 1 $mm^{-3}\ K^{-1}$ occurs at an undercooling which is almost independent of the CE_{99} value. This curving corresponds to a temperature at nearly constant ΔT_L^{gra} value. However, because of graphite growth during further cooling below this temperature, the solidification path reaches the austenite liquidus at a higher and higher temperature as the alloy's CE_{99} value is increased which again disagrees with Figure 3.

Calculations with the 2D—nucleation/lateral growth model were carried out with the same CE_{99} values as

Table I. Values of the Parameters Used for Simulations

V/A (m)	$\sqrt{\Delta}$ (J m^{-2} K^{-1} s$^{-0.5}$)	$C_{p_l}^{liquid}$ (J K^{-1} kg^{-1})	$C_{p_l}^{solid}$ (J K^{-1} kg^{-1})	ρ^{liquid} (kg m^{-3})	ρ^{γ} (kg m^{-3})	ρ^{gra} (kg m^{-3})	ΔH^{gra} (J kg^{-1})
0.009	728	920	750	6800	7000	2200	$1.62 \cdot 10^6$

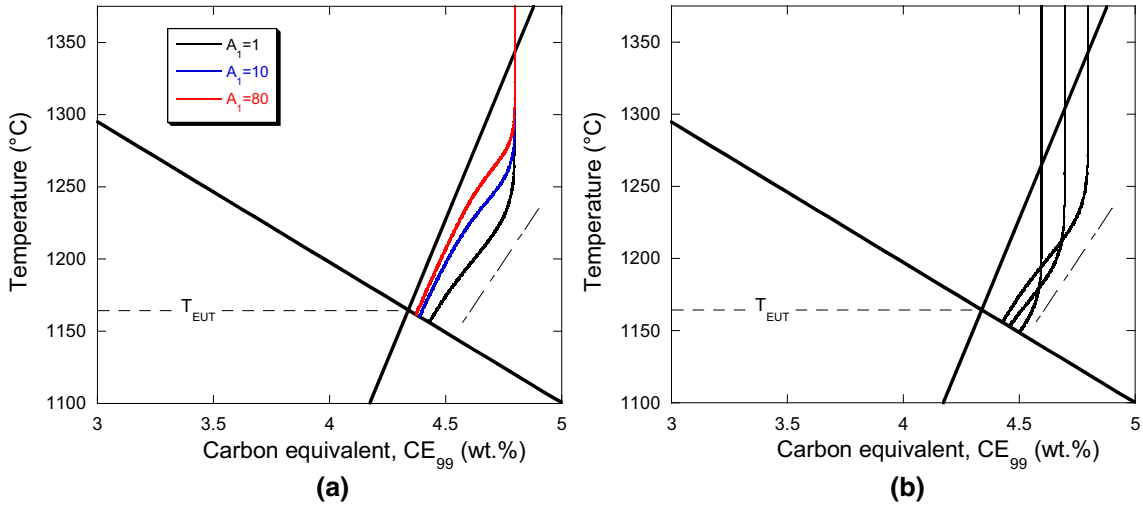

Fig. 8—Solidification path of highly hypereutectic alloys shown in the CE_{99}-T plane. (*a*) calculations for CE_{99} = 4.8 wt pct and three values of the nucleation constant A_1 (mm^{-3} K^{-1}) as indicated in the caption. (*b*) calculations for A_1 set equal to 1 mm^{-3} K^{-1} for three starting values of CE_{99} (4.6, 4.7 and 4.8 wt pct). In both graphs, the dashed line represents the thermal arrest for Mg-treated alloys as in Fig. 2. The bold solid lines are the austenite and graphite liquidus (Eqs. [1] and [2]) calculated for 2.6 wt pct Si.

Table II. Output of Calculations Using Various Values of CE_{99} (wt Pct) and A_1 (mm^{-3} K^{-1}) According to the "Classical" and 2D Nucleation/Lateral Growth Models

CE_{99}	A_1 = 1	A_1 = 10	A_1 = 40	A_1 = 80
"Classical" Model				
4.6	N_V = 85 mm^{-3} g^{gra} = 0.3 pct			
4.7	N_V = 90 mm^{-3} g^{gra} = 0.77 pct			
4.8	N_V = 95 mm^{-3} g^{gra} = 1.2 pct	N_V = 706 mm^{-3} g^{gra} = 1.32 pct		N_V = 4290 mm^{-3} g^{gra} = 1.36 pct
2D—Nucleation/Lateral Growth Model				
4.6	N_V = 117 mm^{-3} g^{gra} = 0.06 pct			
4.7	N_V = 118 mm^{-3} g^{gra} = 0.49 pct			
4.8	N_V = 120 mm^{-3} g^{gra} = 0.84 pct	N_V = 1110 mm^{-3} g^{gra} = 0.89 pct	N_V = 4200 mm^{-3} g^{gra} = 0.91 pct	

above and with A_1 at 1, 10 and 40 mm^{-3} K^{-1} to span the same range of nodule count. The solidification paths are shown in Figure 9 and the main output values are also listed in Table II. It is first seen in Figure 9 that the solidification path curves at about the same undercooling with respect to the graphite liquidus whichever is the CE_{99} value. More important, it is noticed that the solidification path of the alloy at CE_{99} = 4.8 wt pct depends very little on the A_1 value. This is directly related to the fact that growth of graphite in this model is triggered by nucleation of new growth blocks at the surface of the spheroids which varies exponentially with the driving force expressed as a function of the undercooling of the liquid with respect to the graphite liquidus ΔT_L^{gra}. The trends shown in Figure 3 are therefore reproduced in the calculations shown in Figure 9 when this was not the case with Figure 8.

The results in Figure 9 are striking: whatever the alloy's CE_{99} value equal to or higher than 4.6 wt pct and whatever the inoculation level (A_1 value) of the cast

iron, the solidification path will reach the austenite liquidus at a temperature 17 °C to 24 °C below the eutectic temperature. The similarity with the experimental results in Figure 3 is worth being stressed and this has been emphasized with the horizontal arrow pointing to the left of the hypereutectic composition domain which is exactly the same as in Figure 3. For a given CE_{99} value, the temperature at which the austenite liquidus is reached increases only little when the inoculation level is increased, in contrast with the results in Figure 8(a). It may thus be stated that the 2D - nucleation/lateral growth model allows retrieving the main features of primary graphite precipitation while the "classical" model does not.

B. *Consequences on the Understanding of TA Records for Mildly Hypereutectic Cast Irons*

If calculations had been made for mildly hypereutectic alloys with CE_{99} in between the eutectic value at 4.34 wt pct and a maximum value slightly lower than 4.6 wt pct, growth of graphite would not have taken place before the austenite liquidus is reached. Accordingly, the austenite liquidus would be reached at a temperature that corresponds to the CE_{99} value of the alloy. It has been seen that the formation of austenite can occur with some undercooling (Figure 4) or may even not be detected (Figure 3). In either case, Figures 3, 4, and 7 suggest that the bulk eutectic reaction of these mildly hypereutectic alloys takes place only when the temperature has decreased to a value which seems independent of the CE_{99} value. This temperature relates to a carbon enrichment of the liquid corresponding to a carbon equivalent of about 4.63 wt pct in Figure 3. In previous modeling approaches, this carbon enrichment was seen as corresponding to an eutectic undercooling high enough for the eutectic to start growing to some extent. It is, however, striking to note that this also corresponds to an undercooling ΔT_L^{gra} which is on the range of value necessary for primary graphite to grow to a significant extent according to the 2D nucleation/lateral growth model. In line with this conclusion, it is worth noting that Bjerre *et al.*[16] observed the first graphite precipitates in their 4D-XRD synchrotron experiments on an hypo-eutectic spheroidal graphite cast iron at an undercooling with respect to the graphite liquidus higher than 100 °C. These findings suggest the following tentative schematic for solidification of mildly hypereutectic alloys.

Figure 9 is reproduced in Figure 10 without the calculated solidification paths. The lower arrow pointing to the right has been located at an eutectic undercooling ΔT_{EUT} = 28 °C. Its intersection with the austenite liquidus is at CE_{99} = 4.62 wt pct. From this, intersection is drawn the vertical dotted line which separates highly hypereutectic cast irons to the right of it from mildly hypereutectic cast irons to the left of it. The undercooling ΔT_L^{gra} at the intersection amounts to 137 °C, high enough for significant growth of graphite from the liquid according to the 2D nucleation/lateral growth model. Primary solidification of alloys with CE_{99} larger than 4.60 wt pct has been seen to end at a temperature nearly insensitive to the CE_{99} value. This is represented with the arrow pointing to the left in Figure 10 which has been located 10 °C above the lower arrow and points to a liquid of composition CE_{99} = 4.53 wt pct. Increase of the inoculation level of the melt and probably also decrease of the Mg content will move it slightly upwards.

A tentative description of solidification of mildly hypereutectic alloys may then be suggested which should be further substantiated in the future with dedicated

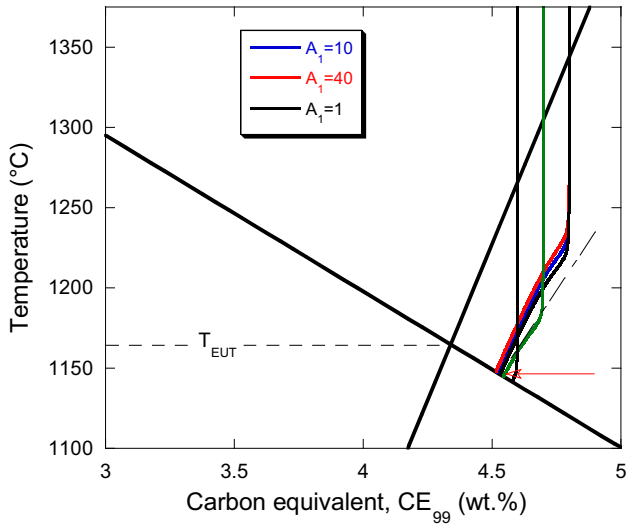

Fig. 9—Solidification path of hypereutectic alloys shown in the CE_{99}-T plane. Calculations for CE_{99} = 4.8 wt pct were performed for three A_1 values, 1, 10, and 40 mm^{-3} K^{-1}. Calculations for CE_{99} at 4.6 wt pct and 4.7 wt pct were carried out with A_1 = 1 mm^{-3} K^{-1}. The bold solid lines are the austenite and graphite liquidus (Eqs. [1] and [2]) calculated at 2.6 wt pct Si. The dashed line represents the thermal arrest for Mg-treated alloys as in Fig. 2.

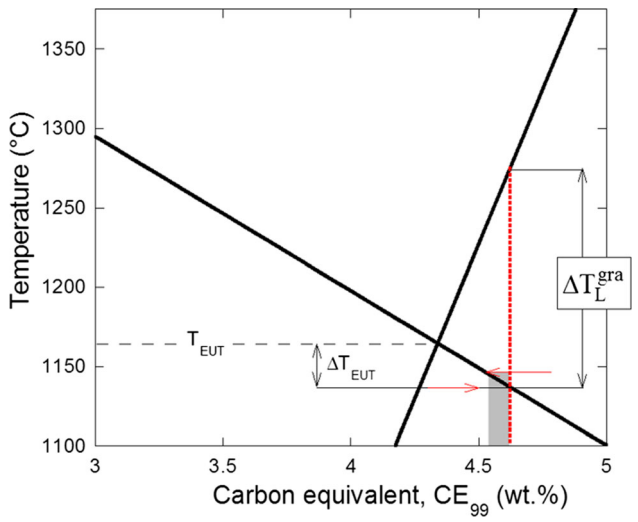

Fig. 10—Schematic showing how to define highly hypereutectic alloys to the right of the vertical dotted line from mildly hypereutectic alloys to the left. The grayed area is the transition zone, see text. The bold solid lines are the austenite and graphite liquidus (Eqs. [1] and [2]) calculated at 2.6 wt pct Si.

experiments. Figure 9 showed that the primary solidification path for an alloy with CE_{99} = 4.6 wt pct is nearly straight, curving only at its bottom end. This means that for alloy's CE_{99} values between 4.34 and 4.60 wt pct, the primary solidification path will be straight down, *i.e.,* no significant growth of primary graphite would have occurred when the austenite liquidus extrapolation is reached. At that temperature, austenite starts forming, possibly with some limited undercooling, and then grows rapidly so that the remaining liquid gets quickly enriched in carbon. With further decrease in temperature, this enrichment is such that the liquid reaches a CE_{99} value corresponding to an undercooling ΔT_L^{gra} high enough for growth of spheroidal graphite, and hence sufficient for the eutectic solidification to start. This straightforward schematic explains that the T_{EU} temperature is constant for near-eutectic hypereutectic alloys.

The transition zone between the two types of hypereutectic alloys may be defined with the grayed area in Figure 10. This area is here drawn for not-inoculated alloys which have been strongly spheroidized, it is expected to move slightly to the left with inoculation and lower Mg treatment. Alloys in this range showed an erratic behavior which has certainly to be related to the efficiency of the nucleation and growth processes of primary graphite. The fact that the formation of austenite is not always detected and this "erratic" primary graphite precipitation might explain the confusion stated by Chaudhari *et al.* when analyzing the TA records of mildly hypereutectic alloys.

IV. CONCLUSION

Detailed analysis of the thermal records of hypereutectic cast irons has evidenced a transition between mildly hypereutectic and highly hypereutectic compositions. Highly hypereutectic alloys often show an arrest that can be associated with primary graphite precipitation and which occurs at a high undercooling with respect to graphite liquidus. Solidification of these alloys then proceeds with a bulk eutectic reaction taking place at a temperature which is nearly insensitive to the carbon equivalent of the alloy. Mildly hypereutectic alloys do not show such a primary arrest and undergo a eutectic reaction that starts at a temperature significantly lower, but yet also independent of their carbon equivalent. This difference has been described as demonstrating the need for the liquid to reach a high enough undercooling with respect to the graphite liquidus for allowing effective graphite growth. This undercooling is reached during primary solidification in the case of highly hypereutectic alloys while it needs that growth of austenite enriches the liquid in carbon in the case of mildly hypereutectic alloys.

Simulation of primary spheroidal graphite precipitation based on a 2D nucleation/lateral growth model has allowed substantiating this distinction between mildly and highly hypereutectic cast irons which have been proposed a long time ago by Chaudhari *et al.* The transition occurs in a limited range of CE_{99} values, namely, 4.53 to 4.62 wt pct for the cooling conditions encountered in standard thermal analysis. Inoculation of the melt shifts this transition to slightly lower CE_{99} values. The very good agreement between predicted trends and experimental results suggests further work in two directions: (1) investigating the effect of cooling rate and magnesium content and (2) extending the analysis to lamellar and compacted graphite cast irons.

ACKNOWLEDGMENT

R.D.C.C. is pleased to acknowledge the support of Fundación Azterlan for performing his PhD research.

APPENDIX A

Tables A-I and A-II list the results selected from the works by Chaudhari *et al.*[6,9] Table A-I gives the reference of the alloys, their carbon, and silicon contents as well as the CE and CE_{99} values for industrial alloys.[9] For those alloys that have been spheroidized, the surface nodule count, N_A, and nodularity are listed when they were reported. For alloys that solidified mostly in the stable system, the N_A values were converted to volume number of graphite particles, N_V, by means of $N_V = \frac{2}{\pi} \cdot \frac{N_A}{\bar{D}_2}$, where $\bar{D}_2$ is the average diameter of these particles in a 2D metallographic section.[22] For doing so, $\bar{D}_2$ was evaluated by setting the area fraction of graphite to an average value g^{gra} = 0.09: $\bar{D}_2 = \left(\frac{4}{\pi} \cdot \frac{g^{gra}}{N_A}\right)^{0.5}$. N_V values are not given for alloys that showed essentially metastable solidification. Table A-II gives the same information for laboratory alloys.[6]

Table AI. Alloy Reference, Carbon and Silicon Contents, Carbon Equivalents CE and CE_{99}, Magnesium Content, Surface and Volume Nodule Counts, and Nodularity for Industrial Alloys[9]

Alloy reference	Pct C	Pct Si	CE	CE_{99}	Pct Mg	N_A (mm^{-2})	N_V (mm^{-3})	Nodularity (Pct)
7T10	3.73	2.02	4.40	4.30	0.061	144	3250	97
7T1	3.75	2.01	4.41	4.31	0.058	140	3120	97
7T4	3.89	1.86	4.51	4.41	0.057	not given		not given
7T11	3.86	2.05	4.54	4.43	0.058	100	1880	93
6T13	3.80	1.91	4.43	4.33	0.055	not given		not given
6T12	3.83	1.89	4.49	4.36	0.053	64	960	89
6T11	3.89	1.96	4.53	4.44	0.056	96	1770	92
6T1	3.81	2.66	4.67	4.55	0.048	not given		not given
4L27	3.72	2.44	4.53	4.40	0.045	190	4930	100
4L17	3.79	2.66	4.58	4.53	0.056	116	2350	99
4L24	3.86	2.55	4.71	4.57	0.048	142	3180	99
4L23	3.96	2.56	4.81	4.68	0.054	173	4280	99
4L18	3.99	2.52	4.83	4.70	0.055	180	4540	99
3L20	3.74	2.53	4.58	4.45	0.058	144	3250	100
6L11	3.78	2.56	4.63	4.50	0.051	144	3250	100
3L31	3.81	2.58	4.67	4.53	0.053	not given		not given
7L11-inoc	3.75	2.63	4.63	4.49	0.057	112	2230	95

In the reference name, T stands for spheroidized and not inoculated, L for spheroidized and inoculated.

Table AII. Alloy Reference, Carbon and Silicon Contents, Carbon Equivalents CE and CE_{99}, Magnesium Content, Surface and Volume Nodule Counts, and Nodularity for Laboratory Alloys[6]

Alloy Reference	Pct C	Pct Si	CE	CE_{99}	Pct Mg	N_A (mm^{-2})	N_V (mm^{-3})	Nodularity (Pct)
1101-base	2.80	2.84	3.75	3.60	—			
1203-base	3.16	2.64	4.04	3.90	—			
1301-base	3.74	2.46	4.56	4.43	—			
2201-base	3.84	2.63	4.72	4.58	—			
1401-base	4.06	2.56	4.91	4.78	—			
2402-base	4.11	2.54	4.96	4.82	—			
1211-Ni-Mg	3.13	2.53	3.97	3.88	0.067	36-mainly carbides		57
1309-Ni-Mg	3.74	2.43	4.55	4.47	0.058	29-mainly carbides		85
2203-Ni-Mg	3.76	2.72	4.67	4.57	0.056	33	360	81
2303-Ni-Mg	3.91	2.60	4.78	4.68	0.055	70	1100	92
1409-Ni-Mg	4.02	2.56	4.87	4.78	0.060	120	2360	100
2407-Ni-Mg	4.07	2.61	4.94	4.85	0.042	107	2210	96
3403-Ni-Mg	4.03	2.34	4.81	4.73	0.060	not given		
3208-inoc	3.42	2.62	4.29	4.20	0.048	67	1030	59

In the reference name has been added "base" for base melts, "Ni-Mg" for spheroidized alloys without inoculation or "inoc" for spheroidized and inoculated alloys. For the spheroidized alloys, the CE_{99} values account for an average of 0.85 wt pct Ni added due to the treatment.

APPENDIX B

Classical Model[17]

The growth rate dr^{gra}/dt of a spherical particle of graphite of radius r^{gra} is related to a carbon flux ϕ from the liquid through the following mass balance:

$$\varphi = -\rho^{gra} \cdot \left(w_C^{gra} - w_C^i\right) \cdot \frac{dr^{gra}}{dt} \qquad [B1]$$

where w_C^{gra} and w_C^i are the carbon content in graphite and in the liquid at the liquid/graphite interface, respectively.

The transfer of carbon to a graphite precipitate proceeds through two steps in series: diffusion in the liquid, on the one hand, and interfacial reaction, on the other hand. Writing that the flux of carbon is the same for these two steps leads to the following equation:

$$-D_C^l \cdot \rho^l \cdot \left.\frac{\partial w_C^l}{\partial r}\right|_{r^{gra}} = -K \cdot \rho^l \cdot \left(w_C^i - w_C^{l/gra}\right)^2 \qquad [B2]$$

where D_C^l is the carbon diffusion coefficient in the liquid, $w_C^l$is the carbon content in the liquid, K the interfacial kinetics constant and $w_C^{l/gra}$ is the liquid carbon content at the equilibrium graphite liquidus.

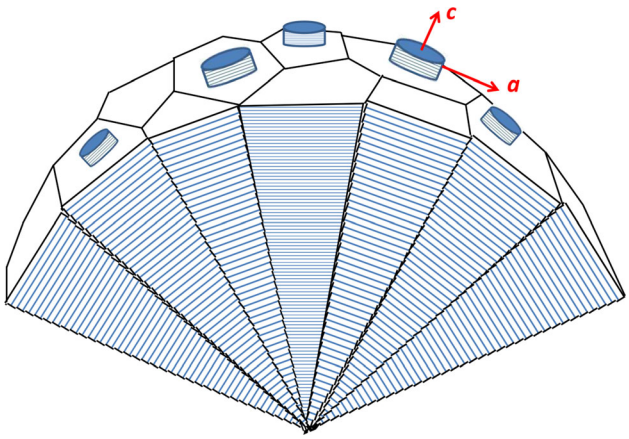

Fig. B1—Schematic of the 2D nucleation/lateral growth model. New growth blocks nucleate in epitaxy at the outer surface of the sectors of the graphite spheroid, and then extend laterally along the prismatic ***a*** direction.

Assuming a steady state carbon profile around the growing graphite nodule, Eq. [B-2] may be solved for w_C^iwhich is then inserted in Eq. [B-1] to give dr^{gra}/dt. Calculations were carried out with an initial nodule radius of 1 μm, $D_C^l = 5 \cdot 10^{-9}$ m^2 s^{-1} and $K = 0.5$ m s^{-1} as previously used.[14]

2D: Nucleation/Lateral Growth Model[21]

In this approach, a spherical shape is assumed which grows by continuous nucleation of new disk-shaped growth blocks at the outer surface of the spheroid on top of the so-called sectors, see Figure B1. The new blocks nucleate in epitaxy or semi-epitaxy with the underlying graphite, and then extend laterally along the surface. The overall growth direction thus remains parallel to the basal ***c*** crystallographic direction of graphite, while growth proceeds in the prismatic ***a*** direction along the outer surface of each sector.

The nucleation rate has been expressed according to Hillig.[23] As suggested by Turnbull and Fisher,[24] the fact that graphite precipitates from an alloy and not from a pure melt may be accounted for by multiplying the nucleation rate for pure melt by the atomic fraction of carbon, x_C. After introduction of appropriate values for the parameters, the nucleation rate J_a was written:

$$J_a \approx 10^{28} \cdot \left(\Delta T_L^{gra}\right)^{1/2} \cdot \beta \cdot \exp\left(-\frac{21500 \cdot \xi}{\Delta T_L^{gra}}\right) \text{ m}^{-2}\text{ s}^{-1} \qquad [B3]$$

where β corrects for structural factors and will be set to 1 as it should be for atoms such as carbon in Fe-C melts, as opposed to molecules for which it may assume higher values.[25] ξ is interface diffuseness which is 1 at most for a sharp interface.[25] In our previous study, a convenient value of ξ was found to be 0.1 which corresponds to an interface thickness of 1.6 atoms according to the computations by Jackson *et al.*[26] for the same case as Cahn *et al.*[25]

The overall growth rate of graphite was then described according to the poly-layer growth (PNG) model already used by Amini and Abbaschian[8] for describing thickening of lamellar graphite plates. The growth rate of a spheroid of radius r^{gra} is thus given as:

$$\frac{dr^{gra}}{dt} = a \cdot \left(\frac{\pi}{3} \cdot J_a \cdot (V_l)^2\right)^{1/3} \qquad [B4]$$

where a is the distance between graphene layers, V_l is the lateral spreading rate of the ledge of the growth block and has been here assumed constant. Assuming this rate is controlled by diffusion of carbon in the liquid, the solution developed by Bosze and Trivedi[27] was adopted. This finally leads to:

$$\frac{dr^{gra}}{dt} = 2.6 \cdot 10^{-11} \cdot \left(\Delta T_L^{gra}\right)^{17/6} \cdot (\beta)^{1/3} \cdot \exp\left(-\frac{7200 \cdot \xi}{\Delta T_L^{gra}}\right) \text{ m s}^{-1} \qquad [B5]$$

in which, as stated above, β will be set to 1 and ξ to 0.1.

The value of x_C that was used to calculate J_a in B-3 was 0.175 which corresponds to $w_C = 4.4$ wt pct, *i.e.*, a slightly hypereutectic alloy in the Fe-C binary system. The same atom fraction corresponds to a strongly hypereutectic alloy in the Fe-Si-C system. It was, however, decided to keep the same expression for J_a as a change of 1.5 at. pct (0.5 wt pct) of carbon leads to a change of about 10 pct of the pre-exponential factor in Eq. [B-5] leading to insignificant change in the result because of the exponential.

REFERENCES

1. A. Dioszegi, V.L. Diaconu, and V. Fourlakidis: *J. Therm. Anal. Calorim.*, 2016, vol. 124, pp. 215–25.
2. D.M. Stefanescu: *Int. J. Metalcast.*, 2015, vol. 9, pp. 7–22.
3. H. Fredriksson and D.M. Stefanescu: Cast Iron Science and Technology*ASM International, OH, ASM Handbook*, 2017, vol. 1, pp. 81–86.
4. D.M. Stefanescu, R. Suarez, and Sung Bin Kim: *China Foundry*, 2020, Vol. 17, pp. 69–84.
5. S. Dawson and P. Popelar: Proceedings of the Keith Millis Symposium, AFS, 2013, pp. 59–66.
6. M.D. Chaudhari, R.W. Heine, and C.R. Loper: *AFS Cast Metals Res. J.*, 1975, vol. 11, pp. 52–60.
7. M. Hillert and V.V. Subba Rao: ISI Publ. 110, The Iron and Steel Institute, London (UK), 1969, pp. 204–12.
8. S. Amini and R. Abbaschian: *Carbon*, 2013, vol. 51, pp. 110–23.
9. M.D. Chaudhari, R.W. Heine, and C.R. Loper: *AFS Trans.*, 1974, vol. 82, pp. 379–86.
10. P. Gustafsson: *Scand. J. Metall.*, 1985, vol. 14, pp. 259–67.
11. R.W. Heine: *AFS Trans.*, 1995, vol. 103, pp. 199–206.
12. M. Castro, M. Herrera, M.M. Cisneros, G. Lesoult, and J. Lacaze: *Int. J. Cast Met. Res.*, 1999, vol. 11, pp. 369–74.
13. J. Lacaze and B. Sundman: *Metall. Trans.*, 1991, vol. 22A, pp. 2211–23.
14. J. Lacaze, G. Lesoult, and M. Castro: *Acta Mater.*, 1998, vol. 46, pp. 997–1010.
15. K.M. Pedersen and N.S. Tiedje: *Int. J. Cast Met. Res.*, 2007, vol. 20, pp. 145–50.
16. M. Bjerre, N.S. Tiedje, J. Thorborg, and J.H. Hattel: *IOP Conf. Ser.: Mater. Sci. Eng.*, 2015, Vol. 84, art. no. 012038.
17. G. Lesoult, M. Castro, and J. Lacaze: *Acta Mater.*, 1998, vol. 46, pp. 983–95.

18. J.A. Dantzig and M. Rappaz: *Solidification*, Engineering Science, EPFL Press, Lausanne, 2009, pp. 268–75.
19. J. Lacaze, M. Castro, N. Aichoun, and G. Lesoult: *Mem. Etudes Sci. Rev. Metall.*, 1989, pp. 85–97.
20. M.A. Azeem, M.K. Bjerre, R.C. Atwood, N.S. Tiedje, and P.D. Lee: *Acta Mater.*, 2018, vol. 155, pp. 393–401.
21. J. Lacaze, J. Bourdie, and M.J. Castro-Roman: *Acta mater.*, 2017, vol. 134, pp. 230–35.
22. M. Coster and J.L. Chermant: *Précis d'analyse d'images*, Presses du CNRS, Paris, France, 1989, pp. 144–48.
23. W.B. Hillig: *Acta metall.*, 1966, vol. 14, pp. 1868–69.
24. D. Turnbull and J.C. Fisher: *J. Chem. Phys.*, 1949, vol. 17, pp. 71–73.
25. J.W. Cahn, W.B. Hillig, and G.W. Sears: *Acta metall.*, 1964, vol. 12, pp. 1421–39.
26. K.A. Jackson, D.R. Uhlmann, and J.D. Hunt: *J. Crystal Growth*, 1967, vol. 1, pp. 1–36.
27. W.P. Bosze and R. Trivedi: *Metall. Trans.*, 1974, vol. 5, pp. 511–12.